Research Square

Preprints are preliminary reports that have not undergone peer review.
They should not be considered conclusive, used to inform clinical practice,
or referenced by the media as validated information.

SERS Chemical Tongue for Rapid Detection of Chili Oils Assisted with a Convolutional Neural Network

Peng Wang
Chongqing Technology and Business University
Cun-Fang Zhang
Chongqing Technology and Business University
Yu Qin
Chongqing Technology and Business University
Xiao-Lan Wei
weishine@ctbu.edu.cn
Chongqing Technology and Business University

Research Article

Keywords: SERS chemical tongue, Convolutional neural network, Chili oil, Capsaicin quantification, Carbonized polymer dots, Food quality assessment

Posted Date: July 27th, 2026

DOI: https://doi.org/10.21203/rs.3.rs-10186586/v1

License: This work is licensed under a Creative Commons Attribution 4.0 International License.
Read Full License

Additional Declarations: No competing interests reported.

Abstract

Chili oil is a widely used condiment, but its complex matrix poses significant challenges for rapid quality assessment. Herein, we develop a surface-enhanced Raman scattering (SERS) chemical tongue by integrating three carbonized polymer dot (CPD)-functionalized magnetic core–silver shell nanoparticles (MNP@Ag-CPDA, MNP@Ag-CPDAB, and MNP@Ag-CPDH) with a tailored convolutional neural network (CNN). The covalently anchored CPDs on the silver surfaces serve as universal receptors—a first for SERS chemical tongues—greatly enhancing sensor stability in the non-polar oil matrix and enabling highly sensitive capsaicin detection with a limit of detection (LOD) of 9.1 ng/mL. The three sensors produced complementary cross-reactive fingerprints, which were concatenated into a super-spectrum and analyzed using a dedicated CNN incorporating parallel max/average pooling fusion, dual output heads for classification and regression, and systematic data augmentation. For pure chili oils, the CNN achieved 100% identification accuracy, outperforming KNN (90.00%), SVM (94.44%), and LDA (99.26%). For complex compounded chili oils involving different oil types, chili varieties, and additives, the CNN maintained 99.63% accuracy and macro F1 score, surpassing KNN (84.44%), SVM (88.15%), and LDA (96.67%). For capsaicin quantification across both simplified and complex matrices, the CNN consistently outperformed PLS-R with higher R^2 values and lower RMSE and MAE, demonstrating superior quantitative accuracy and robustness against matrix interference. This work demonstrates that the synergistic integration of CPD-based universal receptors and a SERS-tailored multi-task CNN enables rapid, accurate, and on-site-ready detection of chili oil and analogous edible oil products.

Introduction

Chili is extensively used worldwide, and its pungency is primarily attributed to vanillamide alkaloids known as capsaicinoids, with nordihydrocapsaicin, homodihydrocapsaicin, and capsaicin being the predominant components [1]. Common chili cultivars in China include Erjingtiao, Chaotianjiao, and Xiaomijiao, which are characterized by mild, moderate, and high pungency, respectively. Even within the same cultivar, the capsaicinoid composition and relative content may vary with the cultivation region and climatic conditions, resulting in distinct differences in pungency and aroma [2]. Most chili peppers are processed into various products such as chili powders, chili sauces, and chili oils. Among these, chili oils are composite condiments made from chili and edible oils, frequently supplemented with auxiliary ingredients like prickly ash and garlic, via extraction, frying, or oil-splashing methods. Their quality depends on the efficient transfer of pungent compounds, pigments, and aroma-active substances from chili and auxiliary materials into the oil, thereby yielding products with harmonious color, aroma, taste, and mouthfeel [3]. Driven by the increasing global consumption of chili and the rapid development of chili-based food products, including chili oil, the global chili and pepper market has continued to expand, with its value estimated at approximately USD 1.3 billion in 2025 and projected to reach USD 1.79 billion by 2030 [4]. Hence, there is an urgent need to develop comprehensive, rapid, and reliable methods for the quality assessment of chili oil to support food production, consumption, and safety, and to further advance the scientization of the food industry.

Current studies address the physicochemical, compositional, and sensory attributes of chili oil, with capsaicinoids as the major target [5, 6]. The detection of capsaicinoids has generally been based on chromatographic separation [7]; however, it requires costly instrumentation and matrix-related pretreatment, limiting its on-site use. Chemical sensors based on molecularly imprinted polymers (MIPs) enable selective quantification [8, 9] but are limited by the availability of specific receptors and are hardly suited for simultaneous detection of multiple analytes. To overcome these issues, a "chemical tongue" or sensor array uses multiple non-specific receptors to generate cross-reactive responses, producing characteristic fingerprints decoded by chemometrics or machine learning [10–14]. This strategy has been applied in environmental monitoring, medical diagnosis, and food analysis [15–17]. For example, Huang et al. [18] developed a dual-signal array using gold nanoparticles and europium-labeled fluorescent microspheres for the rapid detection of aflatoxin B1, benzo(α)pyrene, and capsaicin in edible oil, achieving an LOD for capsaicin of 0.01 ng/mL. Among optical sensors, surface-enhanced Raman scattering (SERS) offers molecular fingerprints with high sensitivity [19, 20] and is well-suited for chemical tongues. Leong et al. [21] and Wei et al. [22] built SERS chemical tongues for wine and Baijiu, but to date, no reports exist on their application to complex foods such as chili oils.

Herein, we present a SERS chemical tongue platform (Fig. 1) with material and algorithmic innovations relative to existing SERS chemical tongues and CNN-assisted spectral analysis: (1) Using carbonized polymer dots (CPDs) as universal receptors. Unlike previous SERS sensor arrays that rely on physically adsorbed or self-assembled small-molecule receptors (e.g., 4-mercaptobenzoic acid, 4-mercaptopyridine), which suffer from ligand desorption and poor stability in oil-rich matrices [23, 24], we introduce CPD-functionalized SERS sensors via in-situ microwave carbonization of aromatic molecules on MNP@Ag. The resulting covalent C–N/Ag and C–O/Ag bonds "lock" the receptors, providing excellent stability in non-polar media. This is the first use of CPDs as non-specific universal receptors in a SERS chemical tongue for a complex food matrix. (2) Tailoring custom CNN architecture to SERS spectral features. Previous CNN-assisted SERS studies either used generic 1D-CNN architectures that ignore the dual nature of SERS spectra (sharp narrow peaks and regionally dense information) or performed only single tasks (classification or quantification) [25–27]. Our CNN introduces: parallel max-pooling and average-pooling followed by summation at the input stage to simultaneously preserve discriminative narrow peaks and overall spectral trends, dual output heads (multi-node for classification, single-node for quantification) to enable integrated qualitative and quantitative analysis, and systematic data augmentation to overcome sample scarcity. Moreover, this work represents the first successful application of a SERS-based chemical tongue to a complex oil matrix (chili oil), which is substantially more challenging than previously analyzed water/alcohol systems (e.g., Baijiu) due to 100% oil phase, high viscosity, and strong background interference. Compared to our own prior work on Baijiu flavors [22], the current platform advances from self-assembled receptors to covalently locked CPDs, from conventional machine learning to a dedicated multi-task CNN, and from an alcohol-water matrix to a pure oil matrix.

Experimental section

Materials and instruments

$FeCl_2·4H_2O$ and absolute ethanol were purchased from Chongqing Chuandong Chemical Group Co., Ltd. $AgNO_3$ was purchased from Chengdu Cologne Chemical Co., Ltd. NaOH was obtained from China National Pharmaceutical Group Chemical Reagent Co., Ltd. 4-Aminothiophenol (ATP), 4-hydroxythiophenol (HTP), benzoic acid (BA), and ethylene glycol were purchased from Shanghai McLean Biochemical Technology Co., Ltd. Capsaicin was obtained from Chongqing Platinum Strontium Titanium Technology Co., Ltd. Rapeseed oil and soybean oil were purchased from Xuyi Shanzhidao Catering Management Co., Ltd. Lard oil and butter oil were purchased from Sichuan Shudongli Supply Chain Management Co., Ltd. Scallion–ginger–garlic oil and Sichuan pepper oil were purchased from Mawang Grain and Oil Co., Ltd. (Zhoukou City, China). The water used in the experiments was deionized water.

TEM images were obtained using an FEI Tecnai G2 F20 microscope. XRD analysis was performed using a Shimadzu XRD-6100 instrument. FTIR analysis was conducted using a Thermo Scientific Nicolet iS20 spectrometer (USA). XPS analysis was performed using a Thermo Scientific K-Alpha spectrometer (USA). Raman spectra were collected using a portable Raman spectrometer ATR3110 from Optosky Photonics Company (Xiamen, China).

Preparation of the SERS chemical tongue

The preparation of MNP@Ag magnetic nanoparticles followed the method of Zhu et al. [28] with appropriate modifications. Briefly, accurately weigh 746 mg of $FeCl_2·4H_2O$ (3.75 mmol, dissolved in 150 mL deionized water, concentration 25 mM) and stir until fully dissolved. Heat the solution to 90°C and rapidly add 10 mL of aqueous NaOH solution containing 400 mg NaOH (10 mmol, 1 M), continue heating for 30 min. Then add 20 mL of aqueous $AgNO_3$ solution containing 425 mg $AgNO_3$ (2.50 mmol, 0.125 M) and stir at 90°C for 1 h. After completion, separate the product using an external magnet, wash three times with ultrapure water, and vacuum dry at 60°C to obtain MNP@Ag magnetic nanoparticles.

Next, weigh 12.02 mg ATP (0.10 mmol) and add to 10 mL anhydrous ethanol, vortex for 5 min until fully dissolved. Add 0.1 g of dry MNP@Ag magnetic nanoparticles, shake and vortex for 1 min, then place in dark for at least 12 h to achieve chemical adsorption equilibrium. Add the mixture to 10 mL of ethylene glycol solution, sonicate at room temperature at 100 Hz for 10 min, then microwave continuously at 252 W for 5 min. Separate the product using a magnet, wash twice with anhydrous ethanol, adjust the volume to 5 mL, and store at 4°C. Repeat the procedure using ATP, BA, or HTP as raw materials to prepare different MNP@Ag-CPDs samples (designated MNP@Ag-CPDA, MNP@Ag-CPDAB, and MNP@Ag-CPDH, respectively). All preparations were performed in triplicate (n = 3 biological replicates).

Performance and characterization of the SERS chemical tongue

To evaluate the enhancement effect of the carbonized MNP@Ag-CPDs magnetic SERS sensor, a 10^{-3} mol/L HTP ethanol solution was prepared and mixed with an equal volume of MNP@Ag-CPDs ethanol solution, followed by incubation for 1 h. Each batch was repeated 15 times with 3 parallel samples per measurement. Raman spectra were recorded using an ATR3110 spectrometer (λ = 785 nm, integration time 10 s, power 10 mW). Prior to measurement, samples were magnetically enriched and washed twice with distilled water. The peak at 1171 cm^{-1} was used to calculate the LOD for the carbonized sensor. The standard deviation σ was determined from 15 blank samples, and a linear calibration curve was constructed using capsaicin concentrations from 0 to 6 μg/mL, with slope S. The LOD was then calculated using the formula LOD = 3σ/S, providing a robust estimate of sensor sensitivity. The enhancement factor (EF) of MNP@Ag-CPDs can be discussed in reference to the non-carbonized MNP@Ag EF data in the Supplementary Materials to illustrate performance improvement. The sensors were further characterized using XRD, TEM, XPS, FTIR, and Raman spectroscopy.

Detection of chili oil samples with the SERS chemical tongue

Chili oil samples include both pure and composite series, covering different base oils, chili types, spiciness levels, and additive combinations. Dried chili powders were cleaned and passed through an 18-mesh sieve. For pure chili oil samples, heat the oil to 180°C, allow it to cool naturally to 160°C, add chili powder at the appropriate ratio, stir for 1 min, and collect the upper layer while hot to cool to room temperature. For composite chili oil samples, mix oil and chili powder at a 2:1 mass ratio, add auxiliary oils at 0.5% of total volume, seal with a film, and maintain in a 90°C water bath for 1 h to fully extract capsaicin. Two parallel batches were prepared for each chili oil formulation, with each batch measured 5 times. Detailed series compositions and recipes, including oil types, chili varieties, additive combinations, and spiciness levels, are provided in Table S1. Commercial chili oil samples were diluted 30-fold before SERS measurement to ensure that the measured capsaicin concentrations fell within the calibration range of 0–6 μg/mL. The final capsaicin contents in the original samples were calculated by multiplying the CNN-predicted concentrations by the dilution factor.

Pattern recognition

This paper designs a CNN model for the qualitative classification of chili oil samples and the quantitative prediction of capsaicin concentration. The overall architecture of the CNN model is illustrated in Fig. 2. For each sample, the Raman spectra collected from the three SERS sensors were concatenated into a one-dimensional SERS super-spectrum and used as the model input. Each super-spectrum was treated as a single-channel one-dimensional input, with a batch input shape of N×1×L, where N is the number of samples, 1 represents the spectral channel, and L denotes the number of wavenumber points.

The network applies max pooling and average pooling in parallel at the input stage. Max pooling is used to enhance sharp and narrow Raman peaks that are important for sample identification, whereas average pooling preserves the global intensity distribution and reduces the influence of local noise. The

outputs of the two pooling branches are then fused, allowing the network to retain both peak-enhanced local information and global spectral trends. After feature fusion, two convolutional feature-learning modules are employed. In the first module, the number of channels is expanded from 1 to 4, and in the second module, from 4 to 8. This gradual increase in channel number improves the model's ability to represent one-dimensional spectral features while maintaining a compact network structure. Both convolutional layers use kernels of length 16 with padding, and each convolutional layer is followed by a ReLU activation function and an average pooling layer. Finally, the extracted features are flattened and fed into a multilayer perceptron. The network contains two output heads: a multi-node output head for multi-class classification of chili oil samples and a single-node output head for regression prediction of capsaicin concentration.

For comparison, PLS-R was applied as a linear chemometric baseline for quantitative analysis, while KNN (k = 5, Euclidean distance), LDA (linear discriminant analysis with full covariance), and SVM (radial basis function kernel, C = 1.0, γ = scale) were utilized as conventional machine-learning baselines for qualitative identification. Quantitative performance was evaluated using the slope and intercept of predicted versus reference values, R^2, root mean square error (RMSE), and mean absolute error (MAE). Qualitative performance was assessed using accuracy, macro precision, macro recall, macro F1, weighted F1, and confusion matrices. To improve statistical rigor, model performance was further evaluated under repeated random splits, and the results were reported as mean ± standard deviation. Learning curves of training and validation losses were also used to monitor the fitting process and to examine whether the CNN showed signs of overfitting.

Results and discussion

Characterization of the SERS chemical tongue

To analyze the structural characteristics of MNP@Ag and the SERS chemical tongue, we characterized them using XRD, TEM, XPS, and FTIR. In the TEM images (Fig. 3A, Supplementary Fig. S1a), all nanoparticles were nearly spherical with good dispersion and uniformity, and the average particle size was approximately 50 nm. Meanwhile, the lattice fringe spacing of MNP@Ag was 0.244 nm, corresponding to the (111) plane of Ag in the HR-TEM image (Fig. 3B). The lattice fringe spacing of MNP@Ag-CPDs was 0.287 nm in Supplementary Fig. S1b, corresponding to the (200) plane of Ag, which is represented by the diffraction peak at 44.5°. This indicates that a film-like structure of carbonized polymer dots (CPDs) formed on the surface of MNP@Ag-CPDs after carbonization. As indicated by the XRD pattern (Fig. 3C), clear diffraction peaks were present at 38.2°, 44.5°, 64.6°, and 77.6°, which match face-centered cubic Ag and are indexed to the (111), (200), (220), and (311) planes. These peaks agree with the standard PDF card of Ag (PDF#99 – 0094) [29]. Additionally, the peaks at 18.3°, 30.1°, 35.4°, 37.1°, 43.1°, 47.1°, 53.4°, 56.9°, and 62.5° correspond to the (111), (220), (311), (222), (400), (331), (422), (511), and (440) planes of MNP, and peaks at 27.4°, 41.2°, 47.9°, 57.0°, 62.6°, and 75.0° correspond to the (002), (102), (112), (220), (311), and (213) planes of C_3N_4. These assignments are consistent with the standard PDF cards of MNP (PDF#89-3854) [30] and C_3N_4 (PDF#87-1526) [31], indicating that low-

temperature microwave carbonization yields a modified surface containing carbon nanostructures and organic components.

In the FTIR spectra (Fig. 3D), characteristic absorption peaks were observed at around 3428 cm^{-1} and 1630 cm^{-1}, attributed to the O–H stretching vibration. Compared with MNP@Ag, the three sensors showed additional characteristic peaks at 2790 cm^{-1} (C–H stretching), 1482 cm^{-1} (benzene ring C = C skeletal vibration), 1083 cm^{-1} (C–O stretching), and 811 cm^{-1} (aromatic C–H out-of-plane bending). Therefore, functional groups such as C–O, C = C, and C–H were formed on the sensor surface after low-temperature microwave carbonization. A comparison of the FTIR spectral characteristics of the functional groups before and after carbonization is detailed in Table S2. Figure 3E shows that the four nanoparticles consist of C, Ag, O, and Fe in the full-resolution XPS spectra. Notably, additional S element peaks appear in the three sensors, attributed to surface sulfur introduction. Figure 3F and Supplementary Fig. S2 show the high-resolution XPS spectra of C, N, and O in the three sensors. The C 1s spectrum resolves peaks corresponding to C–C/C = C, C–O, and C = O bonds. The N 1s spectrum reveals two chemical states, assigned to metal–N and C–NH_2 groups. The O 1s spectrum exhibits signals from both organic C–O structures and metal–oxygen bonds. XPS analysis reveals that functional groups such as C–C, C–O, C = O, C–N, and –C = C– are present on the surface of all three sensors. However, differences in the types and contents of these functional groups are observed among the sensors, with detailed proportions listed in Table S3. In summary, the XRD, TEM, XPS, and FTIR characterization results demonstrate significant differences between the prepared MNP@Ag-CPDs chemical tongue and MNP@Ag in both physical and chemical structures, confirming the successful fabrication of the MNP@Ag-CPDs-based SERS chemical tongue.

Response performance of the SERS chemical tongue

To evaluate the performance of the carbonized MNP@Ag-CPDs magnetic SERS sensors, HTP was used as a probe molecule. SERS spectra of 10^{-3} mol/L HTP solution with MNP@Ag-CPDs were measured, with 15 repetitions per batch and 3 parallel samples per measurement. As shown in Supplementary Fig. S4, the MNP@Ag substrate showed a concentration-dependent SERS response toward HTP over 10^{-10}–10^{-4} mol/L. The intensity at 1074 cm^{-1} exhibited a good linear relationship with − log[c], with $R^2 = 0.997$, indicating reliable quantitative response capability. Moreover, the RSD values of 15 repeated measurements and 15 independent batches were 1.97% and 1.68%, respectively, demonstrating good signal repeatability and batch-to-batch reproducibility. The limit of detection (LOD) at 1171 cm^{-1} was calculated using a 0–6 μg/mL capsaicin calibration curve and the 3σ/slope method (σ = 0.0028 from 15 blank measurements), yielding 0.0091 μg/mL, reflecting sensor sensitivity under practical sample conditions. The EF of the non-carbonized MNP@Ag substrate was calculated using HTP as a probe molecule, and the detailed calculation is provided in the Supplementary Materials (Supplementary Fig. S3). For batch-to-batch reproducibility, MNP@Ag-CPDA was measured at 1078 cm^{-1} and 1171 cm^{-1} across 15 independent batches, showing RSD < 2%, indicating excellent consistency between batches (Supplementary Fig. S5). The stability of a single batch of MNP@Ag-CPDs was monitored over 0–28

days at 1078 cm^{-1} and 1171 cm^{-1}, with RSD < 2%, indicating stable performance (Supplementary Fig. S6). To demonstrate the advantage of the sensor array, PLS-R calibration plots comparing single and multi-sensor arrays are shown in Supplementary Fig. S7, illustrating improved quantification accuracy and repeatability for the array.

Figure 4 displays Raman spectra of the SERS chemical tongue. Characteristic peaks (see Table S4) confirm the successful surface modification of MNP@Ag with sulfur-containing aromatics. MNP@Ag-CPDA exhibits a dominant peak at 1171 cm^{-1} (C–H bending) [33]. MNP@Ag-CPDH and MNP@Ag-CPDAB show the strongest peaks at 1076 cm^{-1} and 1078 cm^{-1}, assigned to C–S stretching coupled with aromatic ring breathing [34]. These peaks differ from the reported 1083 cm^{-1} peak for aminobenzenethiol [32], likely due to new functional groups formed during low-temperature microwave carbonization, which enabled controlled tuning of the sensor surface. These intra-molecular vibrations are stable against external interference, serving as reliable internal standards to correct signal fluctuations. The Raman characteristic peaks of specific groups from these aromatic compounds can be used to track the interactions between the sensors and the flavor components in chili oil.

Response mechanism of the SERS chemical tongue

To clarify how the SERS chemical tongue responds to chili oil flavor components, we examined the interactions between aryl-functionalized sensors and representative analytes and the resulting spectral changes of the immobilized aromatics. Unsaturated fatty acids (USFA), saturated fatty acids (SFA), and capsaicin were used as model compounds (Table S5). After reaction with each component, the SERS spectra were compared by tracking terminal-group-related peaks against the internal standard peaks, as shown in Fig. 5.

First, for the hydroxyl aromatic sensor MNP@Ag-CPDH, the Raman peak at 1167 cm^{-1} corresponding to the O–H bending vibration was selected as the characteristic peak for analysis. As shown in Fig. 5A, the intensity of this peak decreased upon addition of flavor components, which was attributed to hydrogen bonding between HTP and flavor molecules, leading to polarization of the O–H bond and reduced vibrational energy [35]. The HTP sensor exhibited differential spectral responses when interacting with different vegetable oils: pure vegetable oils such as rapeseed oil and soybean oil, being rich in fatty acids, caused a change in the polarization direction of O–H due to the electron-withdrawing effect of carboxyl groups opposing the electron-donating effect of acyloxy/hydroxyl groups, resulting in decreased Raman intensity. The experimental results indicate that mixed vegetable oils had a more significant impact on the sensor spectrum compared with single vegetable oils, which is speculated to arise from the stronger combined effects of interactions among different fatty acids in the mixed oils on the sensor.

Second, for the aryl-modified sensor (MNP@Ag-CPDAB) synthesized via low-temperature microwave carbonization, its interaction with flavor components is primarily achieved through hydrophobic interactions [36]. Studies have shown that the hydrophobic effect may involve the synergistic

contribution of hydrogen bonding and π–π interactions, but the overall interaction strength is much weaker than that of hydrogen bonding [37]. In the Raman spectrum, the C–C stretching vibration peak at 1558 cm^{-1} (Fig. 5B) exhibited an increasing trend upon the addition of flavor components. This phenomenon is closely related to the content of unsaturated fatty acids in the sample: the lower the content of C = C nonpolar bonds, the stronger the polarity of the components, which instead weakens the SERS enhancement effect on the Ag surface, leading to a decrease in signal intensity; conversely, the higher the content of unsaturated bonds, the weaker the polarity of the components, and the more significant the SERS enhancement. These results indicate that the strength of hydrophobic interactions between the sensor and flavor components is regulated by the content of unsaturated fatty acids, thereby influencing the final Raman signal response.

Finally, as shown in Fig. 5C, the introduction of flavor components significantly increased the intensity of the SERS characteristic peak at 1432 cm^{-1} for the amino-containing aryl-modified sensor (MNP@Ag-CPDA). This peak is attributed to the characteristic vibrational mode of p,p'-dimercaptoazobenzene (DMAB), a dimer formed from aniline induced by laser irradiation [38]. This enhancement is speculated to stem from the promoting effect of flavor compounds on dimer formation: the flavor molecules capture hot electrons generated by the decay of surface plasmons, allowing the remaining holes to oxidize the adsorbed ATP molecules, thereby facilitating the generation of DMAB [39]. Meanwhile, the SERS characteristic peak of ATP at 1558 cm^{-1}, corresponding to the C = C stretching vibration of the benzene ring, significantly decreased in intensity upon the addition of flavor components. This change can be attributed to the increased polarization of the aromatic ring resulting from DMAB formation, which reduces the energy required for its vibration. Overall, the composition-dependent spectral changes of the aryl-functionalized sensors indicate that the SERS chemical tongue captures characteristic signatures from complex mixtures, and the interaction analysis provides a mechanistic basis for chili oil identification and discrimination.

Spectral enhancement and training settings for the CNN model

The multi-response signals of the SERS-based chemical tongue were integrated by acquiring spectra from each sample using three distinct sensors, namely MNP@Ag-CPDA, MNP@Ag-CPDAB, and MNP@Ag-CPDH. After standardized preprocessing, the three sensor-response spectra were concatenated into a composite SERS super-spectrum as the model input. Representative super-spectrum profiles for the nine series are presented in Supplementary Fig. S8, where the super-spectra provide an intuitive overview of the overall spectral fingerprints and their inter-series differences. PCA was further performed on the super-spectrum dataset to visualize the similarities and separations among samples in a reduced-dimensional space, and the corresponding score plot is shown in Supplementary Fig. S9.

Data augmentation was introduced to improve the robustness of CNN learning under limited sample size and potential class imbalance. As illustrated in Fig. 6A, the augmentation strategy was designed to

simulate realistic perturbations commonly encountered during SERS measurements. Specifically, Gaussian noise was added to the spectra to mimic random instrumental fluctuations, circular wavenumber shifts of up to 20 cm^{-1} were applied to simulate slight spectral displacement, and linear or slight quadratic baseline drift was introduced to imitate background variation. This procedure expanded the dataset by a factor of ten. After augmentation, negative values were removed using non-negative truncation. The augmented spectra therefore provided more diverse spectral inputs and helped the CNN learn robust features against noise interference, baseline fluctuation, and small peak shifts.

The data splitting and augmentation procedures were carefully controlled to reduce the potential risk of information leakage. The original spectra in each class or concentration level were first randomly divided into training, validation, and test sets at a ratio of 4:3:3. This random splitting procedure was repeated five times with different random seeds to assess the robustness of the validation strategy. In each repetition, data augmentation was conducted separately within each subset. Therefore, all augmented spectra derived from one original spectrum remained in the same subset as their source spectrum, and no augmented variants of the same original spectrum appeared simultaneously in the training, validation, and test sets. The augmented training set was used for CNN parameter learning, the augmented validation set was used for hyperparameter selection and training monitoring, and the augmented test set was used only for final performance evaluation. Under this protocol, each augmented spectrum in the test set was treated as an individual spectral input for evaluating the model performance under realistic spectral perturbations. The final performance metrics were reported as mean ± standard deviation over the five repeated random splits.

The effect of data augmentation was assessed from both model-performance and spectral-pattern perspectives. As shown in Fig. 6B, the CNN models trained with data augmentation achieved higher and more stable classification performance than those trained without augmentation in both series 4 and series 9. This result indicates that the augmentation strategy improved the robustness of CNN-based classification, especially for complex chili oil samples with more diverse spectral variations. Meanwhile, the SERS heatmaps before and after data augmentation were compared to examine whether the augmented spectra preserved the intrinsic spectral characteristics. Figure 6C and Fig. 6D present the heatmaps of series 4 and series 9, respectively, and additional SERS heatmaps before and after data augmentation are provided in Supplementary Fig. S10. The main vertical band patterns remained in the same wavenumber regions after augmentation, indicating that the characteristic Raman peaks were preserved. At the same time, the broader intensity distribution and richer local texture increased within-class variability without introducing obvious spurious peaks. These results suggest that data augmentation increased spectral diversity while maintaining the chemically meaningful Raman fingerprint information.

The CNN was trained on a platform equipped with an Intel Xeon Gold 5218 CPU, an NVIDIA RTX 4090 GPU, and a Python 3.9 environment. The Adam optimizer was used to optimize the model parameters. The learning rate was initially set to 1×10^{-3} and then reduced stepwise by a factor of 10, ultimately selecting an optimal value of 1×10^{-4}. Repeated random splits were further performed to assess the

robustness of the validation strategy, and the corresponding performance variations were summarized using mean ± standard deviation. Supplementary Fig. S11 records the training iteration curves of the CNN across the nine SERS datasets. The training and validation losses showed similar downward trends and stable convergence within 200 iterations, indicating effective model learning and no obvious overfitting.

Chemical tongue detection of simple chili oil

To perform quantitative analysis within simplified chili oil matrices, pure rapeseed oil and a binary vegetable oil mixture (rapeseed and soybean oil, 1:1 v/v) were used to prepare series 1 and series 2 samples at eight capsaicin concentration levels. Figure 7A shows the correlations between the predicted and actual concentrations, and the detailed numerical results are summarized in Table S6. In both series, the CNN achieved higher R^2 values and lower RMSE and MAE than PLS-R, indicating better fitting accuracy and lower prediction errors for capsaicin quantification. Specifically, for series 1, the CNN achieved an R^2 of 0.991, RMSE of 0.205, and MAE of 0.153, outperforming PLS-R with an R^2 of 0.985, RMSE of 0.260, and MAE of 0.200. For series 2, the CNN also showed better quantitative performance, with an R^2 of 0.978, RMSE of 0.312, and MAE of 0.213, while PLS-R obtained an R^2 of 0.961, RMSE of 0.418, and MAE of 0.331. Compared with PLS-R, the CNN regression results were closer to the ideal diagonal, suggesting that the nonlinear model captured concentration-dependent spectral variations more effectively. This advantage was particularly meaningful because even simplified chili oil matrices contain oil-derived background signals that may affect SERS responses. The superior performance of the CNN therefore indicates its ability to extract useful spectral features from the multi-sensor SERS super-spectra and reduce the influence of matrix-related variations. Overall, the SERS chemical tongue integrated with the CNN enabled reliable capsaicin quantification in simplified chili oil systems, providing a basis for subsequent analysis in more complex matrices.

Qualitative identification was further conducted from two perspectives, namely oil matrix type and chili pepper variety, corresponding to series 3 and series 4. CNN, KNN, LDA, and SVM were trained and evaluated under the same preprocessing procedure. The confusion matrices are shown in Fig. 7B,C, and the classification metrics are summarized in Table S7. For both series, the CNN achieved perfect classification, while the other models showed different degrees of misclassification. LDA and SVM also obtained relatively high performance in some cases, suggesting that the SERS chemical tongue generated distinguishable spectral fingerprints among different simplified chili oil samples. However, KNN showed a more obvious performance decrease, indicating that simple distance-based classification was less tolerant to subtle spectral variations caused by oil matrices or chili pepper differences. Compared with these conventional models, the CNN exhibited stronger feature-learning ability by extracting local Raman peak information and global spectral patterns from the concatenated super-spectra. These results demonstrate that the SERS chemical tongue combined with the CNN provides robust qualitative identification for simplified chili oil samples under different oil matrix and formulation conditions.

Chemical tongue detection of complex chili oil

For the quantitative analysis of complex chili oil, this study used rapeseed oil as the base and blended it with one or both of two types of animal oils to formulate binary or ternary blended oil systems. These systems were subsequently mixed with capsaicin at eight concentration levels to prepare the samples for series 5 and series 6. Figure 8A illustrates the correlation between predicted and actual values along with the linear regression fits, while Table S6 details the numerical results. To further evaluate the quantitative reliability of the CNN model in different matrices, an apparent recovery analysis was conducted using representative test samples with known capsaicin concentrations, and the results are summarized in Table S8.

For series 5 and series 6, the CNN consistently achieved higher R^2 values and lower RMSE and MAE than PLS-R, indicating better fitting ability and lower prediction errors in complex chili oil matrices. In series 5, the CNN achieved an R^2 of 0.979, RMSE of 0.306, and MAE of 0.219, whereas PLS-R obtained an R^2 of 0.889, RMSE of 0.699, and MAE of 0.533. In series 6, the CNN also showed better quantitative performance, with an R^2 of 0.977, RMSE of 0.321, and MAE of 0.226, compared with PLS-R with an R^2 of 0.947, RMSE of 0.485, and MAE of 0.383. In particular, the performance gap between CNN and PLS-R became more obvious in series 5, where the matrix composition was more complex. This result suggests that the linear PLS-R model is more susceptible to matrix-induced spectral interference, whereas the CNN can better capture nonlinear spectral variations from the SERS super-spectra. Apparent recovery results further support the quantitative reliability of the proposed method in different chili oil matrices (Table S8). For commercial sample validation, seven chili oil samples were diluted 30-fold before SERS measurement, and the final capsaicin contents were obtained after dilution correction. The corrected results were compared with HPLC values, and spiked recovery tests were further conducted (Tables S9 and S10).

Matrix effects are inevitable in chili oil analysis because different edible oils and auxiliary ingredients may alter the adsorption behavior, local polarity, hydrophobic interactions, and SERS enhancement environment of capsaicin and related compounds. Compared with the simple oil systems, the complex matrices in series 5 and series 6 introduced stronger background variation and nonlinear spectral interference. The superior performance of CNN over PLS-R indicates that the CNN model has stronger robustness against matrix effects and is more suitable for capsaicin quantification in complex chili oil systems. The apparent recovery results further support the quantitative reliability of the proposed method in different chili oil matrices.

This study used three multi-class datasets, namely series 7 to series 9, to evaluate the qualitative performance of the SERS chemical tongue coupled with the CNN. These datasets were designed to reflect variations in oil quality, auxiliary materials, and pungency levels. Under a unified preprocessing procedure, the CNN was compared with KNN, LDA, and SVM. The confusion matrices are presented in Fig. 8B–D, and the accuracy, macro precision, macro recall, macro F1, and weighted F1 are summarized in Table S7.

For series 7 and series 8, the CNN achieved perfect classification performance, while LDA and SVM also obtained high accuracy in most cases. For the more complex series 9, the CNN still maintained a near-perfect accuracy of 99.63%, slightly outperforming LDA and clearly exceeding KNN and SVM. These results indicate that the SERS chemical tongue generated highly distinguishable spectral fingerprints for different chili oil samples, even under the combined effects of oil matrices, auxiliary materials, and pungency differences.

Reliability and interpretability of CNN model

The interpretability of CNN-based recognition can be understood from the spectral response mechanism of the SERS chemical tongue. Although the CNN model automatically learns discriminative features from the concatenated SERS super-spectra, these features are closely associated with chemically meaningful Raman regions. The characteristic bands related to C–S stretching, C–C stretching, O–H bending, C–H bending, and aromatic ring vibration reflect the surface functional groups of the MNP@Ag-CPDs sensors and their interactions with chili oil components. In particular, the –OH functionalized sensor responds to flavor components through hydrogen-bond-related spectral changes, while the MNP@Ag-CPDAB sensor mainly reflects hydrophobic interactions and possible π–π interactions. In addition, the $–NH_2$ functionalized sensor shows DMAB-related spectral variations induced by flavor molecules. These chemically meaningful spectral differences provide an interpretable basis for CNN-based sample discrimination.

From the model perspective, the proposed CNN architecture was also designed according to the characteristics of one-dimensional SERS spectra. The parallel max-pooling branch emphasizes sharp and narrow Raman peaks that are important for sample identification, whereas the average-pooling branch preserves the global spectral intensity distribution and reduces sensitivity to local noise. After feature fusion, the convolutional modules further extract local spectral patterns from the SERS super-spectra. Therefore, the CNN model captures both local peak variations and global spectral trends. Since the input super-spectrum integrates complementary responses from MNP@Ag-CPDA, MNP@Ag-CPDAB, and MNP@Ag-CPDH, the learned features reflect the combined chemical fingerprint generated by the three-sensor chemical tongue. These results indicate that CNN-based recognition is not merely a black-box classification process, but is supported by chemically interpretable SERS fingerprint differences.

Table 1
Comparison with existing works on SERS chemical tongue (ref. 21, 22)

Aspect	Existing works	This work
Food matrix / Target	Simple water and alcohol liquids / Simple, limited categories	Chili oil – high viscosity, strong background interference / Complex, multiple categories: chili × oil × additive
Material innovation	Physical adsorption or self-assembled small-molecule receptors; high risk of desorption	CPD functionalization – covalent bonding to surface; greatly enhancing sensor stability
CNN innovation	No CNN, or generic 1D-CNN not tailored to SERS bands; single task	Dual-branch first pooling (max + avg then sum); multi-task output (classification + regression); systematic data augmentation
Performance	Not reported for oils	Higher classification accuracy, exceeding KNN, SVM, and LDA; higher R^2 and lower RMSE/MAE than PLS-R

Conclusion

In this work, a SERS-based chemical tongue was developed for the rapid characterization of chili oil by integrating a CPD-functionalized multi-sensor array with a custom-tailored multi-output CNN architecture. Three complementary sensors, namely MNP@Ag-CPDA, MNP@Ag-CPDAB, and MNP@Ag-CPDH, provided stable and cross-reactive molecular fingerprints in complex oil matrices, enabling effective characterization of chili oil samples. The specifically designed CNN, featuring parallel max/average pooling fusion, dual output heads, and systematic data augmentation, achieved superior performance over conventional models including KNN, SVM, LDA, and PLS-R. It achieved 100% classification accuracy for pure chili oil and 99.63% accuracy for the most complex chili oil samples in Series 4 and Series 9. For capsaicin quantification, the CNN consistently achieved higher R^2 values and lower RMSE and MAE than PLS-R in both simplified and complex chili oil matrices, demonstrating stronger quantitative accuracy and robustness against matrix interference. As summarized in Table 1, the synergistic integration of material design and algorithmic modeling provides a feasible solution for rapid detection and characterization of chili oil and analogous edible oil products. Future research will focus on: (1) expanding the sample library to include chili oils from different geographic origins and industrial production conditions; (2) validating the method against reference chromatographic methods (HPLC) for regulatory acceptance; and (3) developing a handheld device incorporating the CNN model for on-site quality assessment.

Declarations

Supplementary Information The supplementary material available includes additional Tables and Figures.

Author contribution PW: investigation, software, and writing; CFZ: methodology, investigation, and writing; YQ: investigation and data curation; XLW: conceptualization, funding acquisition, and writing.

Funding Declaration This study was supported by grants from the National Natural Science Foundation of China (31770113) and the Chongqing Natural Science Foundation (CSTB2022NSCQ-MSX1373).

Competing interests The authors declare no competing interests.

References

1. Liu M, Hu L, Deng N et al (2024) Effects of different hot-air drying methods on the dynamic changes in color, nutrient and aroma quality of three chili pepper (Capsicum annuum L). Food Chem X 22:101262. https://doi.org/10.1016/j.fochx.2024.101262
2. Wang N, Zhou X, Zhang T et al (2025) Capsaicin from chili peppers and its analogues and their valued applications: an updated literature review. Food Res Int 208:116034. https://doi.org/10.1016/j.foodres.2025.116034
3. Bai X, Wan P, Liu J et al (2023) Investigation on the changes of carotenoids and capsaicinoids in chili oil at different frying temperature by using ^{1}H NMR. Curr Res Food Sci 6:100411. https://doi.org/10.1016/j.crfs.2022.100411
4. Mohd Ali M, Khalid NI, Wondi MH et al (2025) Exploring the nutritional values, volatile compounds, health benefits, and potential food products of chilli (Capsicum annuum): A comprehensive review. Food Chem 490:145091. https://doi.org/10.1016/j.foodchem.2025.145091
5. Zhu Y, Li X, Jiang S et al (2023) Multi-dimensional pungency and sensory profiles of powder and oil of seven chili peppers based on descriptive analysis and Scoville heat units. Food Chem 411:135488. https://doi.org/10.1016/j.foodchem.2023.135488
6. Barbero GF, Ali L, Latifa A et al (2016) Capsaicinoid contents in peppers and pepper-related spicy foods. Int J Food Prop 19:485–493. https://doi.org/10.1080/10942912.2014.968468
7. Perucka I, Oleszek W (2000) Extraction and determination of capsaicinoids in fruit of hot pepper Capsicum annuum L. by spectrophotometry and high-performance liquid chromatography. Food Chem 71:287–291. https://doi.org/10.1016/S0308-8146(00)00153-9
8. Wang Z, Sheng W, Jin Z et al (2025) Dual network CMCS/PNIPAM temperature-sensitive hydrogel based fluorescent and RGB colorimetric dual-mode immunosensor for detection of capsaicinoids as an exogenous index in edible oil samples. Chem Eng J 521:166601. https://doi.org/10.1016/j.cej.2025.166601
9. Wang J, Yu X, Zhao H et al (2025) Specific and sensitive detection of capsaicin for edible oils authentication using fluorescent molecularly imprinted silica particles. Food Chem 486:144632. https://doi.org/10.1016/j.foodchem.2025.144632
10. Zheng L, RJA, SKS (2019) The optoelectronic nose: colorimetric and fluorometric sensor arrays. Chem Rev 119:231–292. https://doi.org/10.1021/acs.chemrev.8b00226

11. Bilal M, Shabbir MA, Iqbal W et al (2025) Innovative advances in colorimetric sensor array technology for food safety and quality assessment: an updated comprehensive review. Food Rev Int 1–26. https://doi.org/10.1080/87559129.2025.2526677
12. Zheng L, SKS (2020) The optoelectronic nose. Acc Chem Res 54:950–960. https://doi.org/10.1021/acs.accounts.0c00671
13. Tomita S, Sugai H (2024) Chemical tongues as multipurpose bioanalytical tools for the characterization of complex biological samples. Biophys Physicobiol 21(3):e210017. https://doi.org/10.2142/BIOPHYSICO.BPPB-V21.0017
14. Patel H, Portilla VG, Shneidman AV et al (2025) Design principles from natural olfaction for electronic noses. Adv Sci 12:2412669. https://doi.org/10.1002/advs.202412669
15. Johnson NAN, Adade SYSS, Ekumah J-N et al (2025) Advances in mechanisms, designs, and applications of colorimetric sensor arrays for food quality control and authenticity verification. Trends Food Sci Technol 160:104999. https://doi.org/10.1016/j.tifs.2025.104999
16. Yu Y, Cao X, Li C et al (2025) A review of machine learning-assisted gas sensor arrays in medical diagnosis. Biosensors 15:548. https://doi.org/10.3390/bios15080548
17. Li T, Zhu X, Hai X et al (2023) Recent progress in sensor arrays: from construction principles of sensing elements to applications. ACS Sens 8:994–1016. https://doi.org/10.1021/acssensors.2c02596
18. Huang X, Zhang Q, Lu B et al (2025) Time-resolved fluorescence/visual dual-readout nanobiosensors for the detection of aflatoxin B1, benzo(α)pyrene and capsaicin in edible oils using a miniaturized paper analytical device. Food Chem 467:142233. https://doi.org/10.1016/j.foodchem.2024.142233
19. Willets AK (2024) Super-resolution surface-enhanced Raman scattering: perspectives on the past, present, and future. ACS Nano 18:27824–27832. https://doi.org/10.1021/acsnano.4c10655
20. Li RJ, Wei SQ, Yin KX et al (2025) Dual-enhanced SERS platform based on AuNRs@ZnO-Ov core-shell nanostructure for ultrasensitive determination of melamine in food samples. Food Chem 503:147778. https://doi.org/10.1016/j.foodchem.2025.147778
21. Leong YX, Lee YH, Koh CSL et al (2021) Surface-enhanced Raman scattering (SERS) taster: a machine-learning-driven multireceptor platform for multiplex profiling of wine flavors. Nano Lett 21:2642–2649. https://doi.org/10.1021/acs.nanolett.1c00416
22. Wei XL, Jiang L, Shi QL et al (2023) Machine-learning-assisted SERS nanosensor platform toward chemical fingerprinting of Baijiu flavors. Microchim Acta 190:207. https://doi.org/10.1007/s00604-023-05794-z
23. Calderon I, Becerril-Castro IB, Zorlu T et al (2024) Plasmonic cross-reactive sensing noses and tongues. ChemPlusChem 89:e202400210. https://doi.org/10.1002/cplu.202400210
24. Peveler WJ (2024) Food for thought: optical sensor arrays and machine learning for the food and beverage industry. ACS Sens 9:1656–1665. https://doi.org/10.1021/acssensors.4c00252

25. Zhang Z, Li H, Huang L et al (2024) Rapid identification and quantitative analysis of malachite green in fish via SERS and 1D convolutional neural network. Spectrochim Acta Mol Biomol Spectrosc 320:124655. https://doi.org/10.1016/j.saa.2024.124655
26. Wang Z, Liang P, Zhai J et al (2025) Efficient detection of foodborne pathogens via SERS and deep learning: an ADMIN-optimized NAS-Unet approach. J Hazard Mater 489:137581. https://doi.org/10.1016/j.jhazmat.2025.137581
27. Joshi R, Adhikari S, Lee D et al (2025) Detection and classification of microplastics in green tea using SERS with gold nanoparticle substrates integrating chemometrics and deep learning. Curr Res Food Sci 11:101235. https://doi.org/10.1016/j.crfs.2025.101235
28. Zhu S, Fan C, Wang J et al (2014) Realization of high sensitive SERS substrates with one-pot fabrication of Ag–Fe_3O_4 nanocomposites. J Colloid Interface Sci 438:116–121. https://doi.org/10.1016/j.jcis.2014.09.015
29. Jiang P, Yu K, Yuan H et al (2021) Encapsulating Ag nanoparticles into ZIF-8 as an efficient strategy to boost uranium photoreduction without sacrificial agents. J Mater Chem A 9:9809–9814. https://doi.org/10.1039/d1ta00386k
30. Zhang J, Shang X, Ren H et al (2019) Modulation of inverse spinel Fe_3O_4 by phosphorus doping as an industrially promising electrocatalyst for hydrogen evolution. Adv Mater 31:1905107. https://doi.org/10.1002/adma.201905107
31. Ghodsi S, Esrafili A, Sobhi HR et al (2021) Synthesis and application of g-C3N4/Fe3O4/Ag nanocomposite for the efficient photocatalytic inactivation of Escherichia coli and Bacillus subtilis bacteria in aqueous solutions. AMB Express 11:161. https://doi.org/10.1186/s13568-021-01324-3
32. Wang Y, Zhang C, Yu R et al (2023) Robust and sensitive determination of nitrites in pickled food by surface-enhanced Raman spectroscopy. Spectrochim Acta Part A: Mol Biomol Spectrosc 309:123794. https://doi.org/10.1016/j.saa.2023.123794
33. Ni Y, Zhang C, Yuan Y et al (2019) Determination on origination of surface enhanced Raman scattering effect on nano ZnO substrate. Acta Chim Sinica 77:641–646. https://doi.org/10.6023/a19040156
34. Yang Y, Zhang Z, Wan M et al (2020) Highly sensitive surface-enhanced Raman spectroscopy substrates of Ag@PAN electrospinning nanofibrous membranes for direct detection of bacteria. ACS Omega 5:19834–19843. https://doi.org/10.1021/acsomega.0c02735
35. Zhang X, Sui H, Wang X et al (2016) Charge transfer process at the Ag/MPH/TiO_2 interface by SERS: alignment of the Fermi level. Phys Chem Chem Phys. https://doi.org/10.1039/c6cp04370d
36. Nemethy G (1967) Hydrophobic interactions. Angew Chem Int Ed 6:195–206. https://doi.org/10.1002/anie.196701951
37. Peng B, Chen L, Que C et al (2016) Adsorption of antibiotics on graphene and biochar in aqueous solutions induced by π-π interactions. Sci Rep 6:31920. https://doi.org/10.1038/srep31920
38. Xu P, Kang L, Mack NH et al (2013) Mechanistic understanding of surface plasmon assisted catalysis on a single particle: cyclic redox of 4-aminothiophenol. Sci Rep 3:2997.

https://doi.org/10.1038/srep02997

39. Liu Y, Yang D, Zhao Y et al (2019) Solvent-controlled plasmon-assisted surface catalysis reaction of 4-aminothiophenol dimerizing to p,p'-dimercaptoazobenzene on Ag nanoparticles. Heliyon 5:e01545. https://doi.org/10.1016/j.heliyon.2019.e01545

Figures

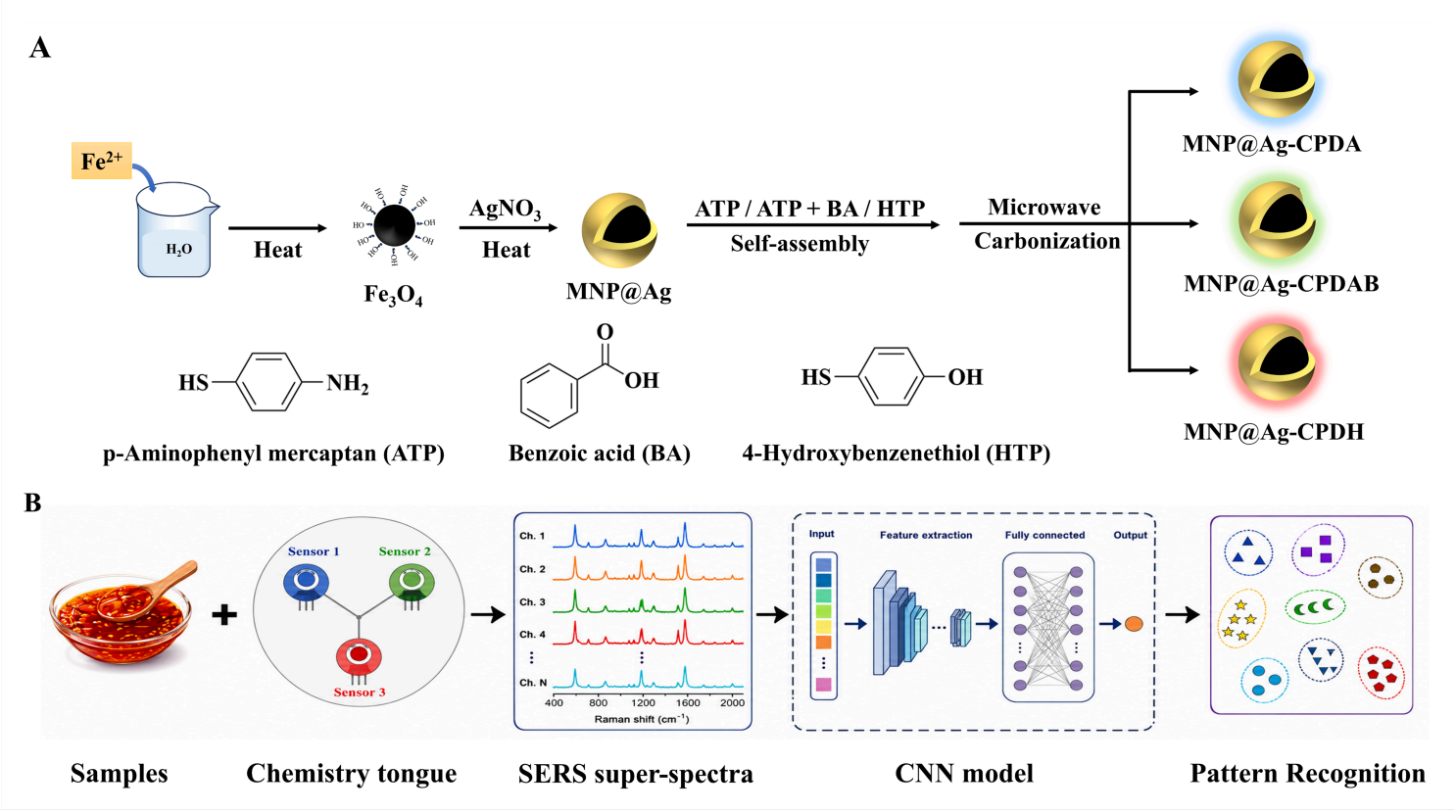

Figure 1

Overview of the SERS chemical tongue platform for chili oil analysis. (A) Fabrication and application process, including synthesis of MNP@Ag nanoparticles, CPD functionalization, sensor array preparation, and SERS measurement of chili oil samples. (B) Signal recognition process, comprising concatenation of three sensor spectra into a super-spectrum, CNN-based feature learning, and dual-output tasks for classification and quantification.

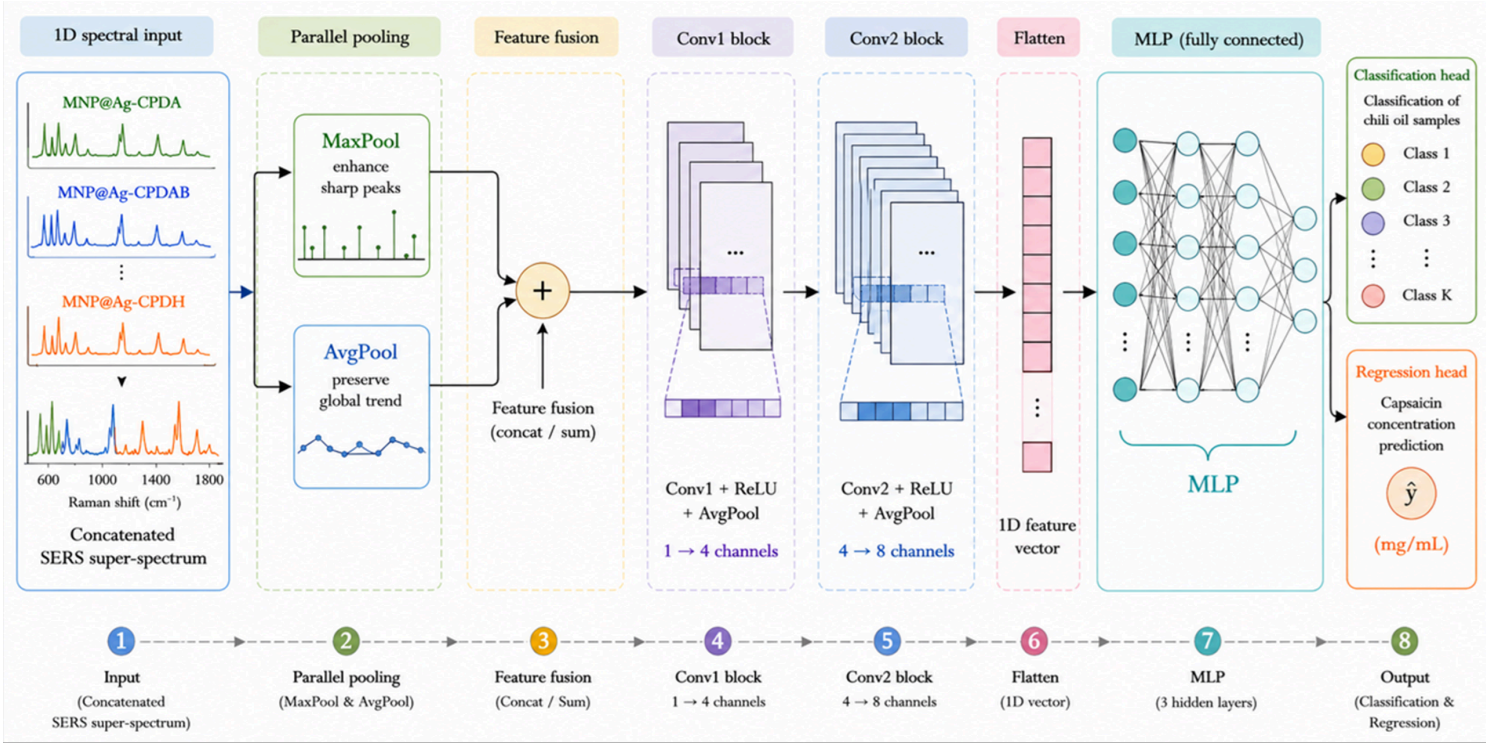

Figure 2

CNN architecture for SERS chemical tongue-based chili oil recognition. The network features parallel max/average pooling fusion at the input stage, two convolutional feature-learning modules with gradually increasing channel numbers (1→4→8), and dual output heads for classification and regression tasks.

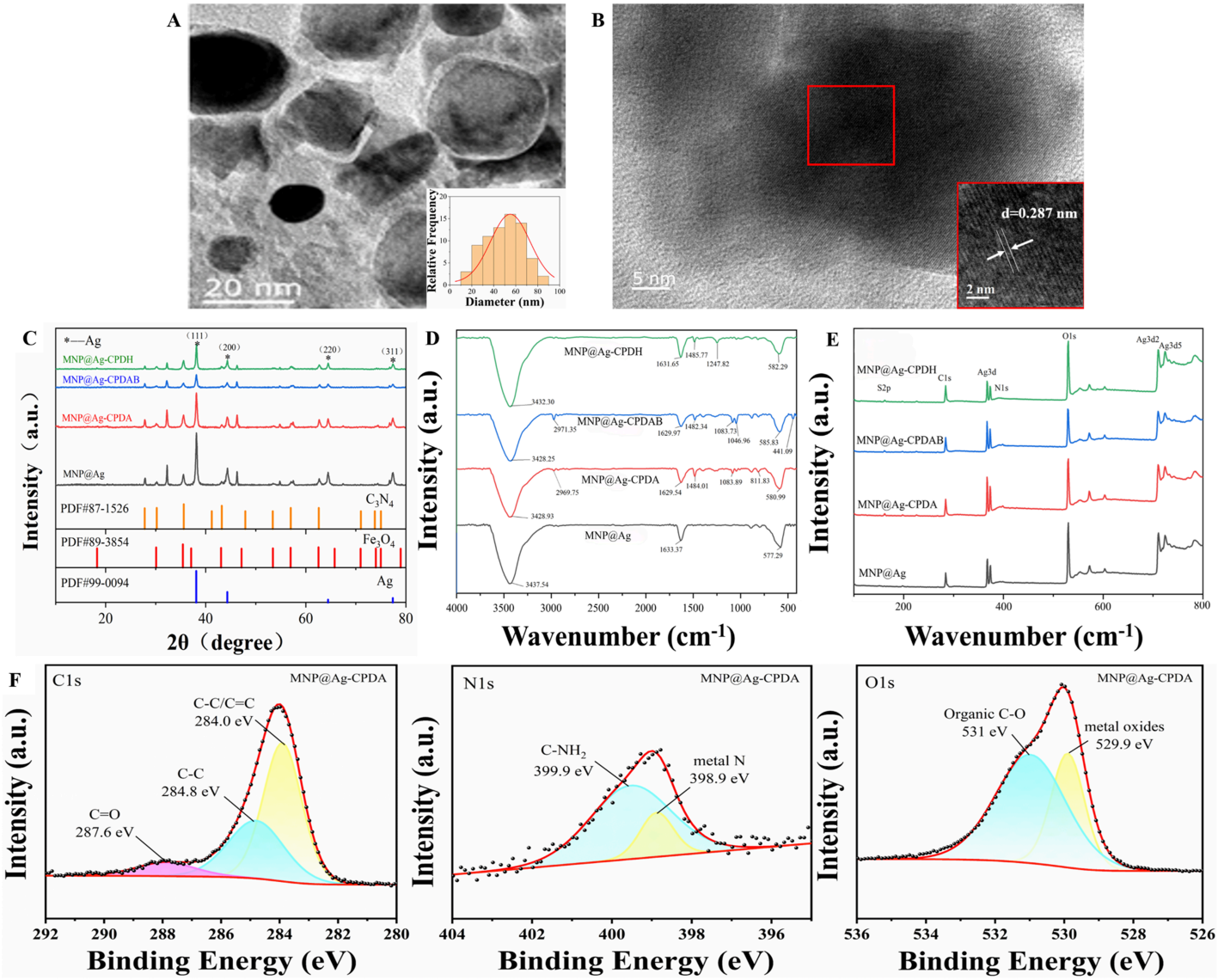

Figure 3

(A) TEM (inset: size distribution) and (B) HR-TEM (inset: lattice spacing) images of MNP@Ag-CPDs. (C) XRD patterns, (D) FTIR spectra, and (E) full-resolution XPS spectra of MNP@Ag and MNP@Ag-CPDs. (F) High-resolution XPS spectra of MNP@Ag-CPDA.

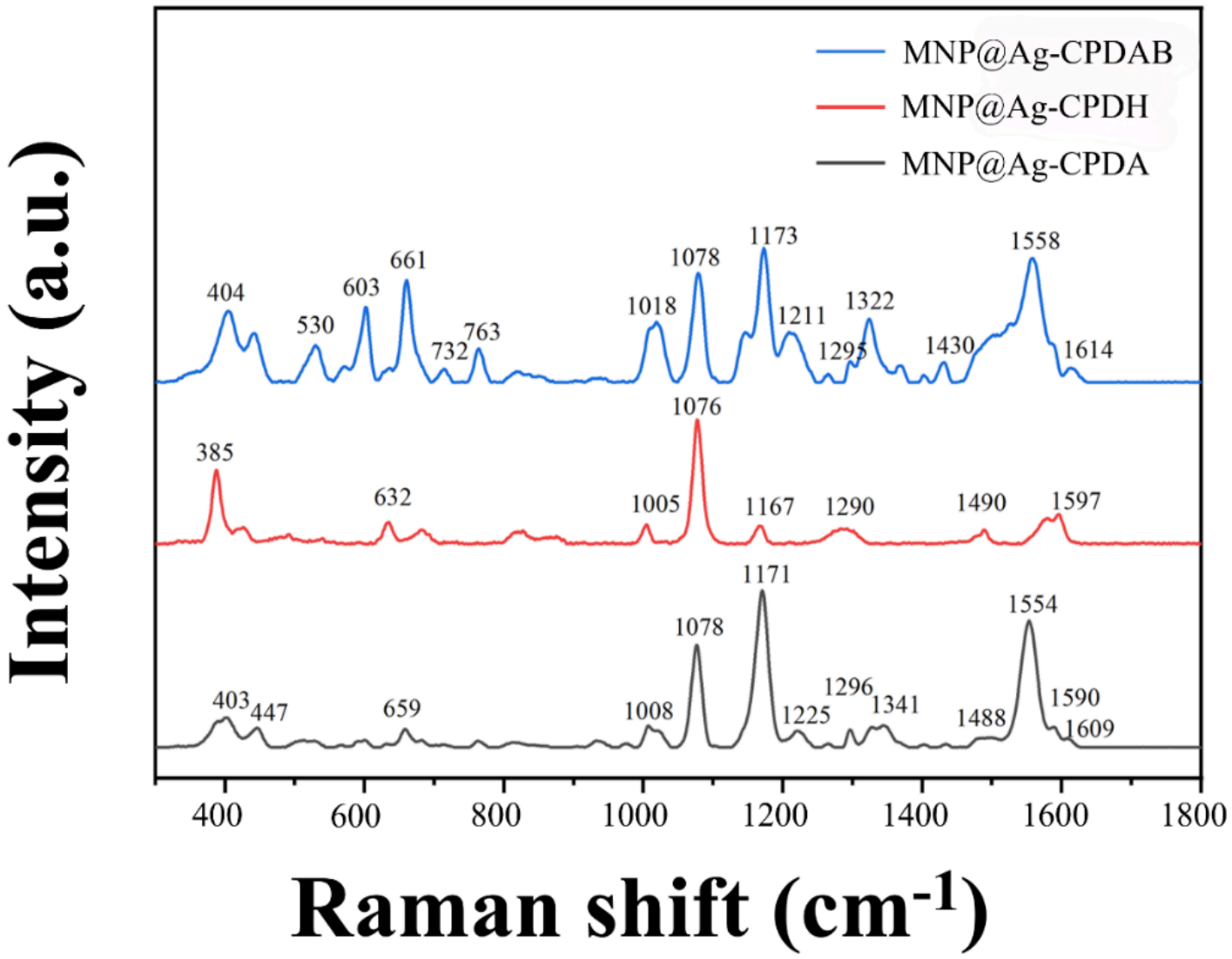

Figure 4

SERS spectra of the SERS chemical tongue (MNP@Ag-CPDA/CPDAB/CPDH).

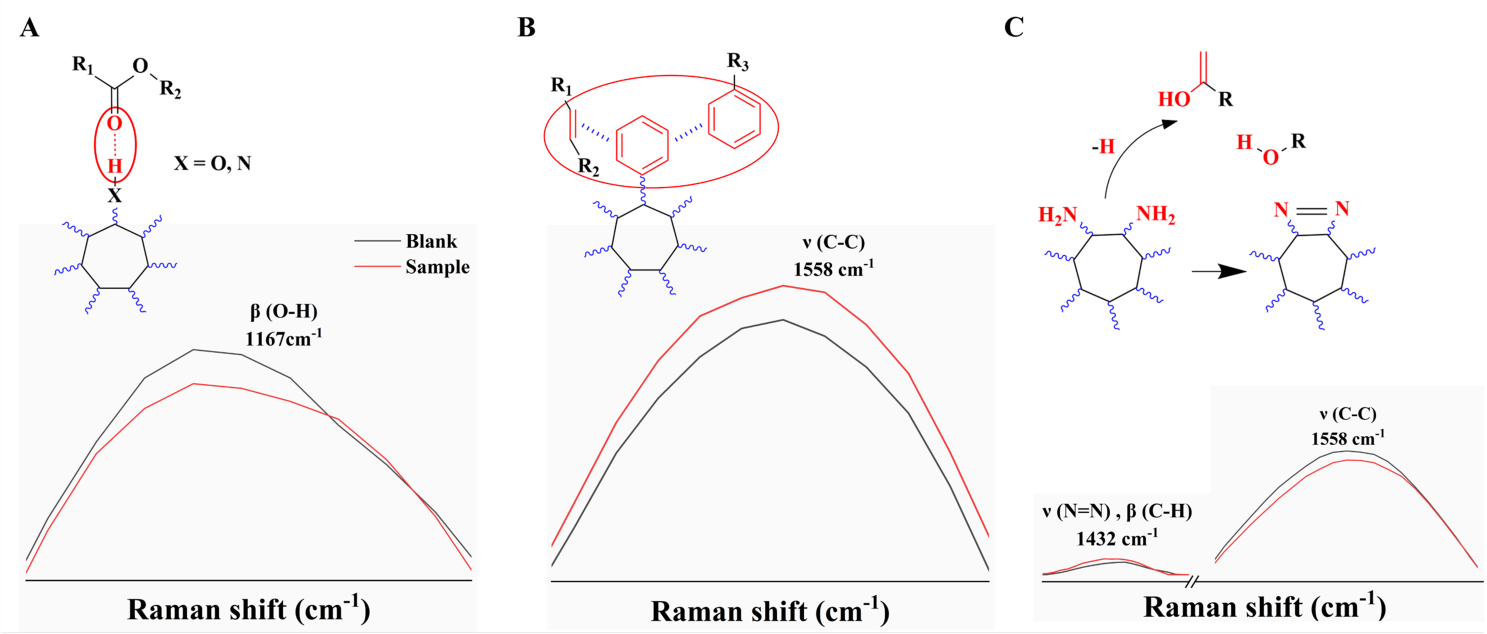

Figure 5

(A) Interaction mechanism and SERS spectra for MNP@Ag-CPDH with flavor components. (B) Interaction mechanism and SERS spectra for MNP@Ag-CPDAB with flavor components. (C) Interaction mechanism and SERS spectra for MNP@Ag-CPDA with flavor components.

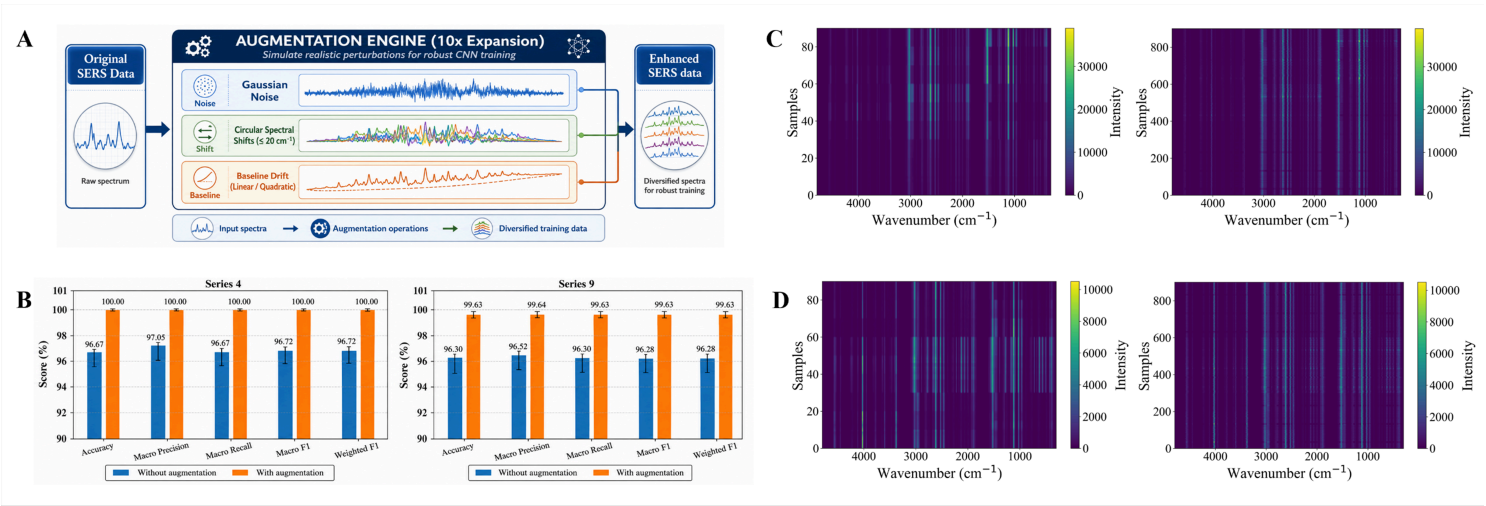

Figure 6

Effect of data augmentation on SERS spectral diversity and CNN performance. (A) Workflow of the data augmentation procedure. (B) CNN performance with and without data augmentation. (C) SERS heatmaps of chili oil series 4 before (left) and after (right) data augmentation. (D) SERS heatmaps of chili oil series 9 before (left) and after (right) data augmentation.

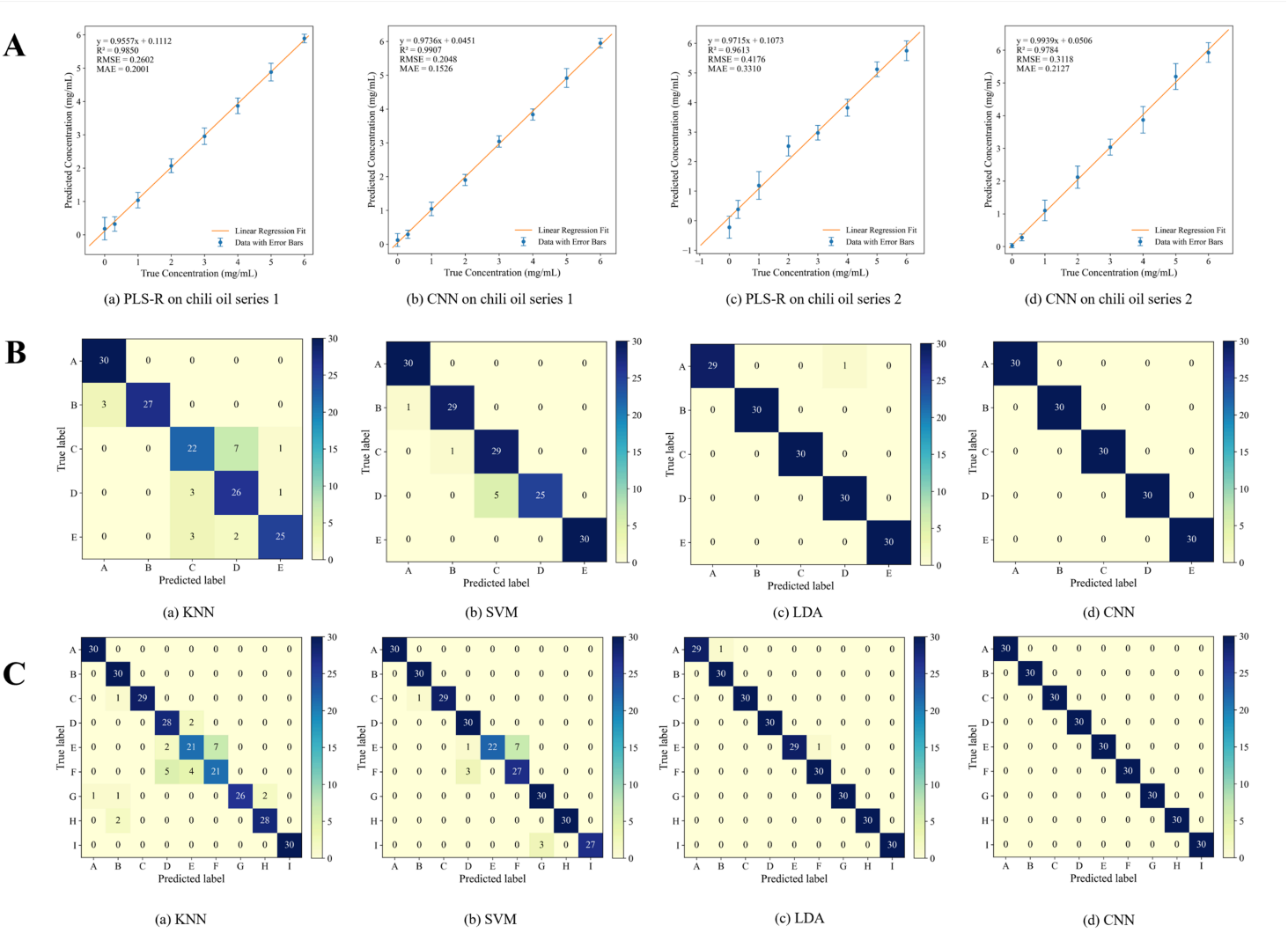

Figure 7

(A) Calibration curves for quantitative analysis of capsaicin in pure chili oil using PLS-R and CNN: (a) and (b) are for chili oil series 1 (RO, capsaicin concentration 0, 0.3, 1.0, 2.0, 3.0, 4.0, 5.0, 6.0 μg/mL), and (c) and (d) are for chili oil series 2 (1 RO : 1 SO, capsaicin concentration 0, 0.3, 1.0, 2.0, 3.0, 4.0, 5.0, 6.0 μg/mL). (B) Confusion matrices for qualitative analysis of the oil matrix in pure chili oil (chili oil series 3, same chili pepper, different oils) using KNN, SVM, LDA, and CNN. (C) Confusion matrices for identifying different pure chili oil samples (chili oil series 4, different oils and chili peppers) using KNN, SVM, LDA, and CNN.

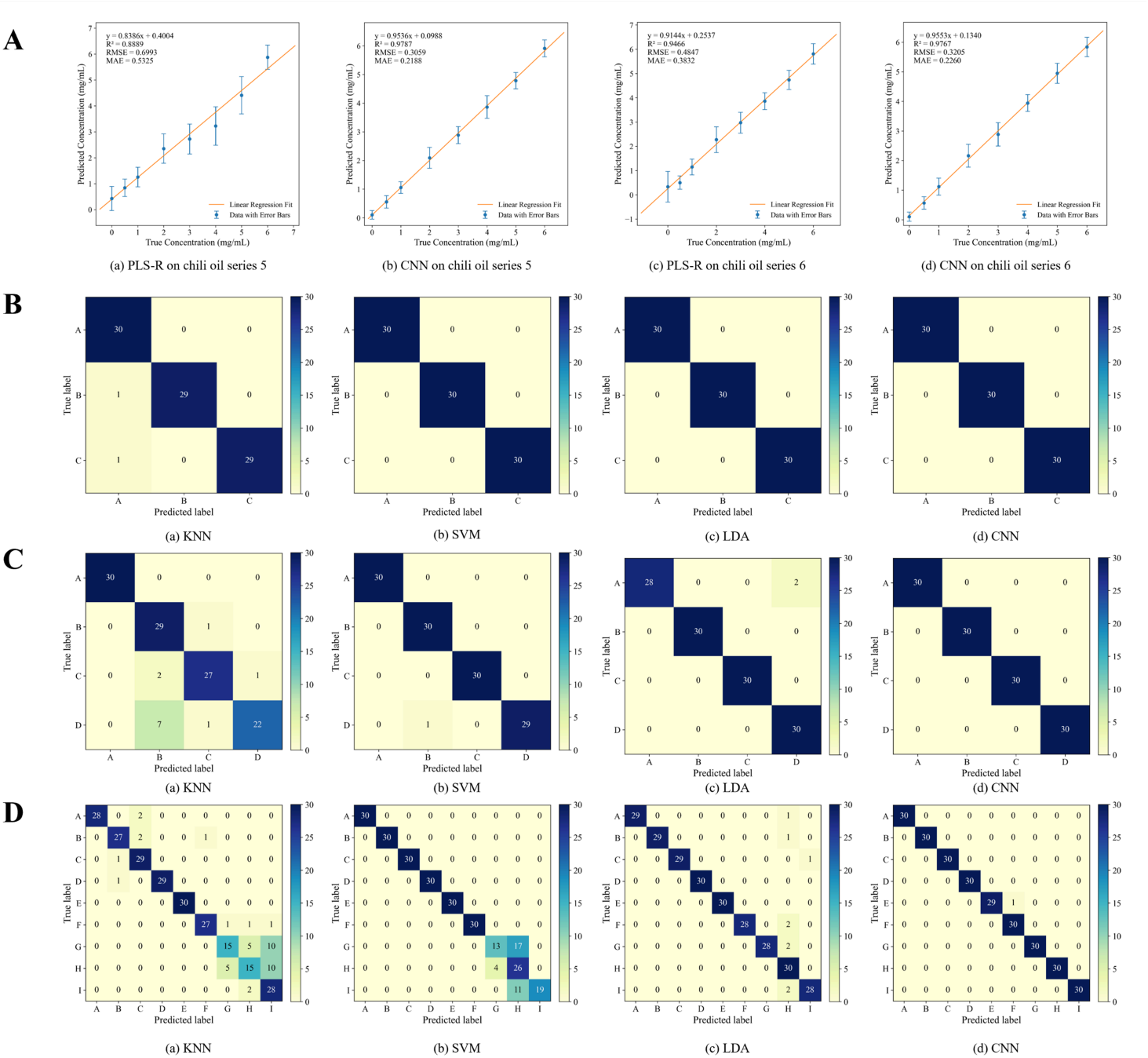

Figure 8

(A) Calibration curves for quantitative analysis of capsaicin in complex chili oils using PLS-R and CNN: (a) and (b) are for chili oil series 5 (1 RO : 3 BT, capsaicin concentration 0, 0.5, 1.0, 2.0, 3.0, 4.0, 5.0, 6.0 μg/mL), and (c) and (d) are for chili oil series 6 (1 RO : 1.5 LO : 1.5 BT, capsaicin concentration 0, 0.5, 1.0, 2.0, 3.0, 4.0, 5.0, 6.0 μg/mL). (B) Confusion matrices for qualitative analysis of the oil matrix in complex chili oil (chili oil series 7, same chili pepper and additives, different oils) using KNN, SVM, LDA, and CNN. (C) Confusion matrices for qualitative analysis of excipients in complex chili oil (chili oil series 8, same oils and chili pepper, different additives) using KNN, SVM, LDA, and CNN. (D) Confusion matrices for identifying complex chili oil samples (chili oil series 9, different oils, additives, and chili peppers) using KNN, SVM, LDA, and CNN.

Supplementary Files

This is a list of supplementary files associated with this preprint. Click to download.

- SupplementaryInformationlegends.docx
- MCASM.docx
- graphicalabstract.jpg